Desalination and Water Treatment
www.deswater.com

doi: 10.5004/dwt.2022.28780

270 (2022) 260–274
September

Adsorptive removal of cationic dyes (methylene blue and crystal violet) from aqueous solutions using anionic polyacrylamide-based monolith

Ayat Allah Al-Massaedh[a,*], Fawwaz I. Khalili[b], Ahmad Al Shra'ah[a]

[a]*Department of Chemistry, Faculty of Science, Al al-Bayt University, 25113 Mafraq, Jordan, email: almassaedh@aabu.edu.jo (A.A. Al-Massaedh) http://orcid.org/0000-0002-2384-9088; email: aalshraah@aabu.com (A. Al Shra'ah)*
[b]*Department of Chemistry, Faculty of Science, The University of Jordan, 11942 Amman, Jordan, email: fkhalili@ju.edu.jo*

Received 11 March 2022; Accepted 27 July 2022

ABSTRACT

In the present study, a macroporous anionic polyacrylamide-based monolith bearing negatively charged binding sites was synthesized as an adsorbent for the efficient removal of cationic dyes including methylene blue (MB) and crystal violet (CV) from aqueous solutions. The effects of various experimental parameters such as solution pH, contact time, monolith dosage, and initial dye concentration on the dyes adsorption were studied using batch experiments. Kinetic studies showed that the adsorption of MB and CV onto the monolith could be better described by the pseudo-second-order kinetic model (R^2 = 1.0). The experimental equilibrium data for CV and MB were best fitted to the Langmuir isotherm model. The maximum monolayer adsorption capacity of the monolith is 120.5 mg g^{-1} for MB and 21.93 mg g^{-1} for CV at 25°C. The adsorption for MB and CV is spontaneous and exothermic. The studies reveal a significant influence of the molecular size of the dye on its percent removal. Reusability investigations indicated that the synthesized monolith could successfully adsorb MB dye after regeneration.

Keywords: Methylene blue; Crystal violet; Polyacrylamide-based monolith; Adsorption; Kinetics; Isotherms; Thermodynamics

1. Introduction

Freshwater is one of the most essential and important needs for a healthy life of human, animal, and plant [1,2]. During the last years, contamination of ground and surface water resources with high levels of toxic organic, inorganic, and biological pollutants was dramatically increased due to rapid and unorganized growth in economics and populations. The industrial effluent containing synthetic dyes is one of the major pollution sources that cause a serious risk to human health [3–6]. The presence of synthetic dyes in water results in several environmental problems such as colored water, increasing toxicity, and reduction in oxygen diffusion through the water surface [4,5,7]. Synthetic dyes with heterocyclic aromatic structure such as methylene blue (MB) and triphenylmethane dyes such as crystal violet (CV) are important commercial dyes that are widely used in various type of industries such as papermaking, printing, food processing, cotton dyeing, leather dyeing, plastic and rubber dyeing, wood preserving chemicals, personal care products, and pharmaceuticals [8–14]. In general, a large percentage (10%–20%) of the synthetic dyes used in the dyeing processes does not effectively bind to the clothes and is directly released into the water system. As a result, huge amounts of toxic synthetic dyes are released into the water system making the industrial effluent highly colored and undesirable [3]. The toxicity of the synthetic dyes stems from the fact that they have a high

* Corresponding author.

chemical and photolytic stability because of their complex unsaturated aromatic structures [14]. Therefore, photo degradation or biological treatment of these dyes is very difficult, leading to their accumulation in the water system [15,16]. Several studies have reported that the long-term exposure to synthetic dyes can cause substantial risks to human health such as vomiting, nausea, eye burns, difficult breathing, profuse sweating, brain confusion, methemoglobinemia anemia, and hypertension [6,16–19].

Different physical and chemical techniques have been widely used for the removal of toxic synthetic dyes from industrial effluents such as chemical precipitation, membrane separation, flocculation, photocatalytic degradation, ozonation, reverse osmosis, solvent extraction, and ion exchange [4,6]. However, these techniques show some limitations like low removal efficiency, consuming a large amount of chemicals, high operational costs, long duration time, and generation of large quantities of toxic products [2,5,6]. In recent years, adsorption has attracted increasing interest as an attractive alternative to these removal techniques for water purification, which is documented in a large number of review articles [2,4–6,20]. This is because of the advantageous adsorption offers over other removal techniques like high selectivity and removal efficiency, simplicity and flexibility of design, availability of a wide variety of adsorbents, easy to regenerate, and low operational cost [6,20,21]. In this context, different types of adsorbents have been used for the removal of toxic synthetic dyes from aqueous solutions including: ultrasound nanoparticles Cu-MOF [22], Zr_3O/activated carbon composite [23], activated carbon prepared from *Ferula orientalis* [24], natural bentonite [25], natural zeolite [16], activated carbons prepared from rice husk [26], activated carbon prepared from palm fibres [27], surfactant-modified alumina [28], resorcinol-formaldehyde carbon xerogels [29], eggshells [21], N-succinyl-chitosan-*g*-polyacrylamide/attapulgite composite [18], biochar/iron oxide composite [12], activated carbon by surfactant modification [8], fennel seed [30], carbon monolith [31–33], silica-based monolith [34], aluminosilicate monolith [35], activated carbon cloth [36], sepiolite [37], magnetic oxidized multi-walled carbon nanotube-κ-carrageenan-Fe_3O_4 nanocomposite [38], and agar/κ-carrageenan composite hydrogel adsorbent [39].

The development of highly crosslinked porous polymer-based and inorganic silica-based monoliths has gained increasing attention due to their ease of preparation, high porosity, high surface area, high adsorption capacity, reusability, and chemical/thermal stability [33,34,40–48]. These advantages make monoliths promising materials that have been successfully used in different applications such as separations, heterogeneous catalysis, adsorption, extraction, pre-concentration, and purification [32–35,40,44,47,49–51]. For example, Sharma et al. [34] synthesized mesoporous silica supported metal-oxide ($ZnO@SiO_2$) monoliths via nanocasting process from macroporous parental silica-based monolith (SiO_2). The formed monoliths were utilized as a promising adsorbent for the efficient removal of pesticides and dyes including Alizarin (AZ), Paradol (PD), Acid Blue-113 (AB) and Rhodamine-B (RD) from aqueous solutions. The authors found that the maximum adsorption capacity of the synthesized silica-based metal-oxide ($ZnO@SiO_2$) monolith is 625, 500, 714 and 555 mg g^{-1} for AZ, RD, AB, and PD, respectively.

In our previous work, we have described the synthesis and characterization of a macroporous anionic polyacrylamide-based monolith bearing negatively charged interaction sites as adsorbent for the removal of heavy metal and radioactive ions from aqueous solutions [40,44]. This is the first study of its kind to investigate the performance of anionic polyacrylamide-based monolith as adsorbent for removal of toxic dyes (MB and CV) from aqueous solutions.

The monolith was synthesized by free radical copolymerization of the soluble inclusion complex (N-tert-butylacrylamide/methylated β-cyclodextrin) with vinylsulfonic acid, piperazinediacrylamide, and methacrylamide in the presence of ammonium sulfate in aqueous phosphate buffer inside a glass tube. The influences of solution pH, contact time, monolith dosage, and initial dye concentration on MB and CV removal were determined. The adsorption kinetic data were modeled by the pseudo-first-order, pseudo-second-order, and Elovich kinetic models. With the aim to understand the adsorption of the investigated dyes onto the synthesized monolith, the Langmuir, Freundlich, Dubinin–Radushkevich, and Temkin adsorption isotherm models were used to describe the equilibrium isotherm data. The adsorption thermodynamic values were evaluated. The regeneration studies were also performed to check the reusability of the synthesized monolith towards MB.

2. Experimental

2.1. Chemicals and instruments

N,N,N′,N′-Tetramethylethylendiamine (TEMED), di-sodium hydrogenphosphate dihydrate, ammonium sulfate (AS), hydrochloric acid (37%, v/v), and methanol were purchased from Fluka (Buchs, Switzerland). Vinylsulfonic acid (VSA) (25% w/v in aqueous solution) and ammonium persulfate (APS) were purchased from Sigma Aldrich (Steinheim, Germany). Methacrylamide (MA), sodium dihydrogen phosphate monohydrate, methylene blue (MB), and crystal violet (CV) were purchased from Merck (Darmstadt, Germany). Piperazinediacrylamide (PDA) was purchased from Alfa-Aesar (Karlsruhe, Germany). Methylated β-CD (Me-β-CD) was purchased from Sigma-Aldrich (Louis, USA). All these chemicals are analytical-grade reagents and used as received without further purification.

The pH of solutions was measured using EUTECH pH-meter (Japan). Sample solutions were shaken using GFL-85 thermostatic mechanical shaker (200 rpm). A 0.45 μm nylon Syringe filters were used to filter the solutions prior to analysis. The absorbance of MB and CV was measured at the maximum absorption wavelength using VIS-spectrophotometer from METASH, model V-5100.

2.2. Synthesis of polyacrylamide-based monolith

The macroporous polyacrylamide-based monolith used in this study was synthesized and characterized as described in [40] by free radical copolymerization of a mixture of *N-tert*-butylacrylamide/methylated β-cyclodextrin, vinylsulfonic acid (VSA), piperazinediacrylamide

(PDA), methacrylamide (MA), ammonium sulfate (AS), ammonium persulfate (APS), and *N,N,N′,N′*-Tetramethylethylendiamine (TEMED) in 0.1 M aqueous phosphate buffer (pH 7.0) inside a glass tube. The glass tube was then closed, and the polymerization process was allowed to proceed overnight at room temperature and then fully characterized. The monolith used in this work was previously characterized by means of thermal gravimetric analysis (TGA) and scanning electron microscopy (SEM) [40].

2.3. Spectrophotometric determination of MB and CV

The chemical structure and chemical formula of MB (319.85 g mol^{-1}, λ_{max} = 609 nm) and CV (407.97 g mol^{-1}, λ_{max} = 590 nm) are shown in Fig. 1. An aliquot of filtrate solution containing MB or CV molecules was quantitatively transferred into volumetric flask and diluted (if necessary). Then, the concentration of unabsorbed dye left in solution was determined at the maximum absorption wavelength using VIS spectrophotometer. After each measurement, the cuvette was rinsed with 0.1 M HCl and water to remove all traces of the dye from previous run.

2.4. Batch adsorption studies

In this study, all batch adsorption experiments for MB and CV were conducted at 298 K in a set of 250 mL plastic stoppered bottles containing 10 mg of the monolith and 25 mL of either MB (50 mg L^{-1}) or CV (10 mg L^{-1}) solution.

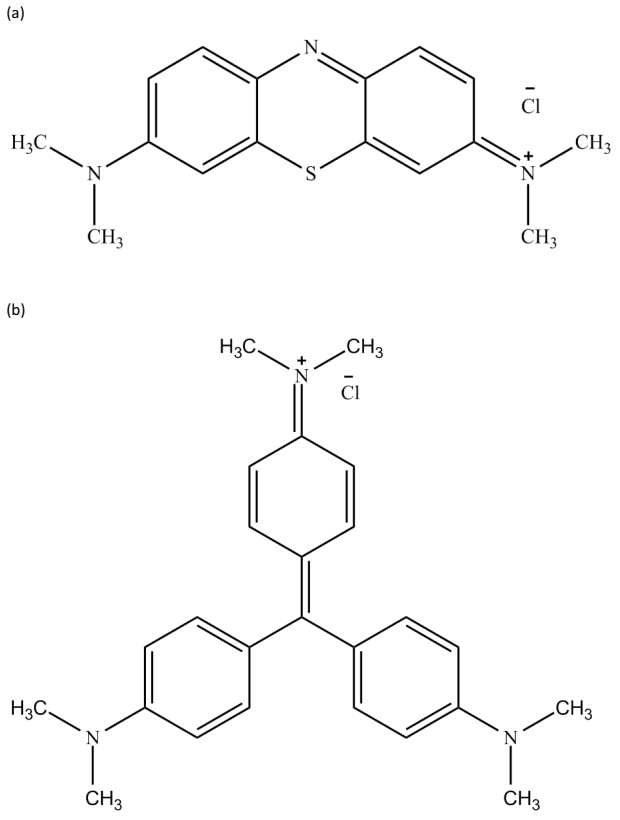

Fig. 1. Chemical structure of (a) MB ($C_{25}H_{30}N_3Cl$) and (b) CV ($C_{25}H_{30}N_3Cl$).

The adsorption experiments were carried out by continuously agitating the dye solution including the monolith at 200 rpm in a thermostatic shaker. Generally, adsorption is affected by various experimental parameters. In this study, the influences of solution pH, monolith dosage, initial dye concentration, and contact time on the removal of MB and CV were investigated. The monolith dosage varied between 5 and 35 mg. After that, a mass of the monolith was mixed with dye solution with different pH range (2–10 for MB) and (3–8 for CV) to optimize pH solution. The adsorption at different time intervals (1, 2, 4, 7, 24, and 48 h) was examined until the adsorption reached the equilibrium.

2.5. Adsorption experiments: kinetics and isotherms

Adsorption kinetic experiments were performed at 25°C, 35°C, and 45°C at pH 5.0 (for MB) or 4.0 (for CV). Suspensions of 10 mg of the monolith in 25.0 mL of 50 mg L^{-1} (for MB) or 10 mg L^{-1} (for CV) solutions were shaken at 200 rpm. At the desired time for each bottle (1, 2, 4, 7, and 24 h), the suspensions were filtered and analyzed by VIS spectrophotometer. Adsorption isotherm experiments were performed at pH 5.0 (for MB) or 4.0 (for CV) at constant temperatures 25°C, 35°C, and 45°C. A mass of 10 mg of the monolith was added to each dye solutions (25.0 mL) of varying initial concentrations (10–100 mg L^{-1}) for MB or (5–25 mg L^{-1}) for CV.

The efficiency of the dyes adsorption was estimated from the calculation of the adsorption capacity at equilibrium q_e and percent removal (%) using the following equations [40]:

$$q_e = \frac{(C_o - C_e)}{m} V \tag{1}$$

$$\%\text{Removal} = \frac{(C_o - C_e)}{C_o} \times 100 \tag{2}$$

where q_e is amount of dye adsorbed per mass unit of monolith at equilibrium (mg g^{-1}), C_o is the initial dye concentration (mg L^{-1}), C_e is the equilibrium dye concentration (mg L^{-1}), m is the mass of the monolith (g), and V is the volume of the aqueous solution (L).

3. Results and discussion

3.1. Adsorption studies

3.1.1. Effect of solution pH

It is well known that the pH of the aqueous solution has a strong impact on the efficiency of the adsorption process by affecting both the surface charge of adsorbent and the degree of ionization of the adsorbate molecule [21,40,45]. As can be seen from Fig. 2a, the percent removal of the studied dyes increases with increasing pH of the dye solution from 2 to 10 and reached nearly a plateau. It can be seen that the maximum percent removal was observed at pH 5.0 for MB (63%) and at pH 4.0 for CV (52%) and further increase in the pH of the dyes solution does not significantly increase the percent removal of the investigated dyes. These findings

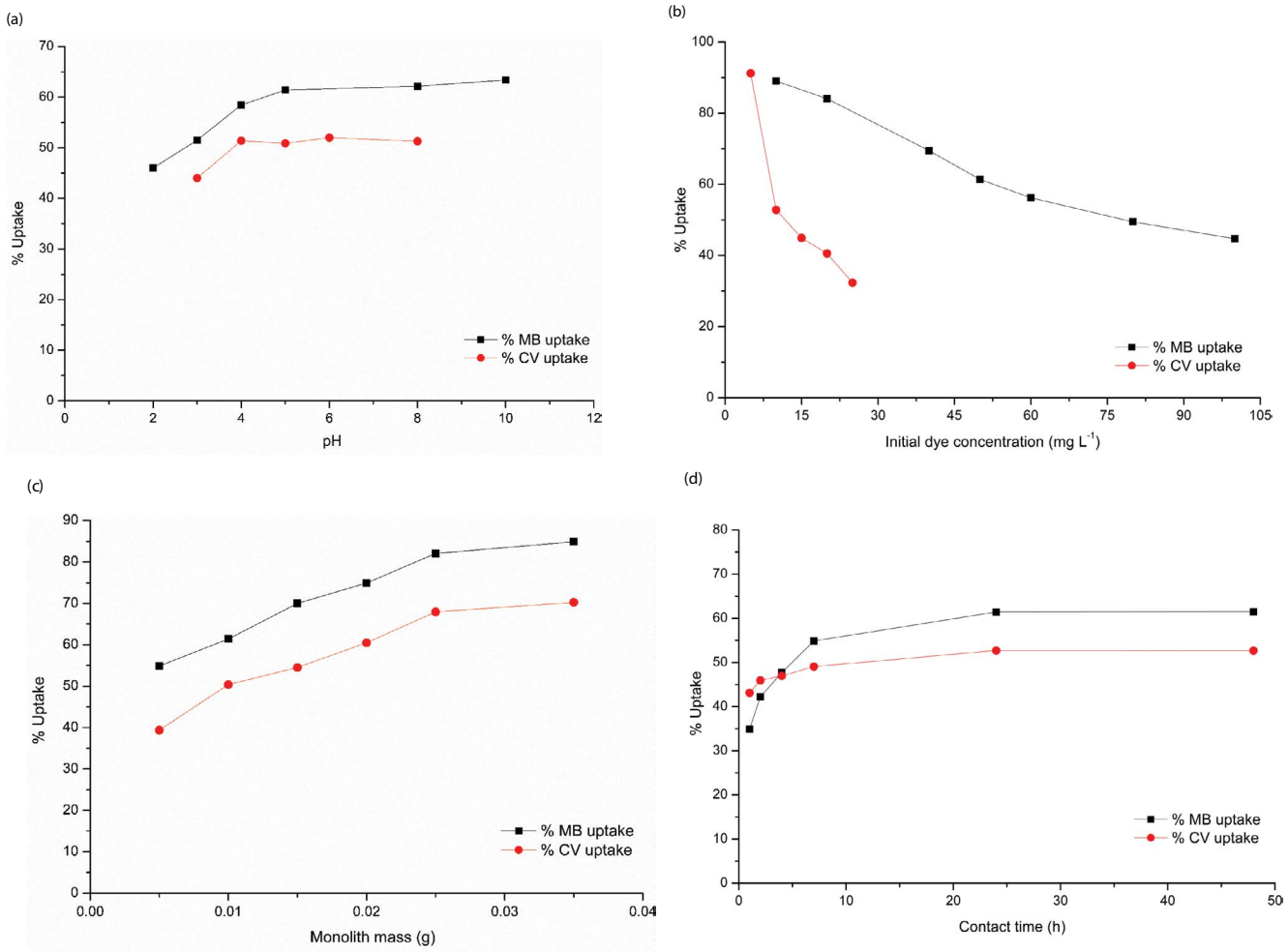

Fig. 2. Effect of various operational parameters on the percent removal of MB and CV dyes including: (a) effect of pH, (b) effect of initial concentration, (c) effect of monolith dosage, and (d) effect of contact time.

can be explained by the increase in the number of the deprotonated negatively charged sulfonate groups per surface unit monolith that form a complex with dye molecules. At low pH values (pH < 5.0 for MB and pH < 4.0 for CV), adsorption occurred with low percent removal for MB and CV. This is because, at low pH, the extremely high concentration of H^+ ions in the aqueous solution covered the monolith surface and results in the generation of positively charged monolith, which restricted dye cations approach to the negatively charged sulfonate groups present on the monolith surface through a strong electrostatic repulsion, and thereby results in low dye removal efficiency [21,43]. As the pH of the dye solution is increased, an increase in the percent removal of the investigated dyes is observed, which might be attributed to the reduction of H^+ ions in the aqueous solution and thus increase in the number of the deprotonated negatively charged sulfonate groups on the monolith surface. Consequently, the electrostatic repulsion between dye cations and H^+ ions on the monolith surface decreases and thereby results in the increase of the dye removal efficiency due to a strong electrostatic attraction between the negatively charged sulfonate groups and the dye cations. Several authors have reported an increase in percent removal of MB and/or CV with increasing the pH of the dye solution using different adsorbents [8,18,21,52,53].

3.1.2. Effect of initial concentration

The influence of initial concentration on the adsorption of MB and CV was studied in the range of (10–100 mg L^{-1}) for MB and (5–25 mg L^{-1}) for CV at 25°C, 35°C, and 45°C. Fig. 2b shows that there is a decrease in the percent removal of MB and CV with increasing their initial concentrations. For example, it was observed that an increase in the initial MB concentration from 10 to 100 mg L^{-1} leads to a decrease in the percent removal from 89% to 45% for MB and from 92% to 30% for CV adsorbed on the monolith. This is mainly because all the available binding sites (i.e., the negatively charged sulfonate groups) on the monolith surface become saturated at higher initial dye concentrations [16,36,50]. In addition, at high initial dye concentrations, the ratio of dye molecules to the monolith mass is high and hence more dye molecules are bonded to the same number of binding sites on the monolith surface, which results in saturation of the monolith surface, and

consequently, decreasing in the percent removal of dye molecules [27,44,54]. Whereas, at low initial dye concentrations, the ratio of dye molecules to the monolith mass is low and hence more dye molecules are adsorbed on the monolith surface due to the availability of binding sites, which in turn leads to an increase in the percent removal of dye molecules. Similar results have been reported for the adsorption of MB and/or CV by different adsorbents [8,21,53].

3.1.3. Effect of monolith dosage

The results obtained in this study confirmed that the monolith dosage has a significant impact on the adsorption processes of MB and CV, since it determines the number of available binding sites, number of pores in the monolith, and surface area available for adsorption. As a general trend, there is an increase in the percent removal of MB and CV with increasing the mass of the monolith from 5 to 25 mg as shown in Fig. 2c. For example, the percent removal of MB increases from about 55% to 82% with increasing the mass of the monolith from 5 to 25 mg. Simillary, the percent removal of CV increases from 39% to 68% with increasing the monolith dosage from 5 to 25 mg (Fig. 2c). The increase in the dyes percent removal with an increase in the monolith dosage is mostly attributed to the availability of more binding sites (i.e., sulfonate groups) on the monolith surface and to increase in the total adsorption surface area available to dye molecules [8,21]. In addition, results show that further increase in the monolith mass (>25 mg) does not significantly increase the percent removal of the investigated dyes, which might be attributed to the fact that at high monolith dosage the available number of the dye molecules in solution was not enough to completely bind with all binding sites (i.e., sulfonate groups) available on the monolith surface [8,21]. Several authors have reported an increase in the percent removal of MB and/or CV with increasing adsorbent dosage [8,21,52,53].

3.1.4. Effect of contact time

Contact time is an important experimental parameter required for studying the adsorption kinetics of MB and CV on the monolith surface. In this study, the influence of contact time on the adsorption of MB and CV was studied between 1 and 48 h. As can be seen from Fig. 2d, the percent removal of MB and CV was increased rapidly within the first 1–7 h (fast adsorption), and then slightly increased until the relative adsorption equilibrium was reached at 24 h (slow adsorption). For example, there is an increase in the percent removal of more than 27% for MB reached during the time interval 1–24 h, which is mainly attributed to the presence of sufficient number of binding sites (i.e., sulfonate groups) on the monolith surface to interact with the dye molecules and to the presence of the large amount of adsorption surface area available for adsorption of the dye molecules [52]. In addition, results show that further increase in contact time (>24 h) does not significantly change the percent removal, indicating that all the available binding sites on the monolith surface become saturated with the dye molecules, and consequently, establishment of equilibrium between the dye molecules adsorbed on the monolith surface and those present in the bulk aqueous solution. Another possible reason that explains the constant percent removal obtained for MB and CV at the later stage (i.e., after 24 h) might be due to the aggregation of dye molecules with the increase in contact time [24]. As a result, the aggregated dye molecules are no longer able to diffuse from the bulk aqueous solution into the pores of the monolith, and thereby results in constant percent removal of the dye [24].

Results in Fig. 2d show that there is an increase in the percent removal of approximately 9% for CV reached during the time interval 1–48 h. The clear difference in the percent removal for MB and CV during the time interval 1–48 h might be directly related to the size of both dye molecule and the pores of the monolith [22]. The small MB molecule enters and leaves the pores of the monolith rapidly and thereby results in the increase of the percent removal of MB, whereas the larger CV molecule enters and leaves the pores of the monolith slowly, which results in a low percent removal of CV [22]. Several authors have reported an increase in percent removal of MB and/or CV with increasing contact time [8,18,21,24,53].

3.2. Adsorption kinetics

The study of the adsorption kinetics is an essential step to evaluate the adsorbent efficiency and to determine the reaction rate constant [55,56]. With the aim to study the rate and mechanism of the adsorption reactions between the investigated dyes and monolith, and to quantify the theoretical equilibrium adsorption capacity, the experimental kinetic data obtained for MB and CV were analyzed using Lagergren pseudo-first-order, pseudo-second-order, and Elovich kinetic models at 25°C, 35°C, and 45°C [55–57]. In the present study, the values of correlation coefficient R^2 and reduced chi-square χ^2 were applied to evaluate the consistency between the experimental kinetic results and the theoretical values of the proposed kinetic model, and consequently, to find out the most suitable kinetic model that can be used for describing the experimental results. In general, the suitable kinetic model used for describing the experimental results is characterized by high R^2 and low χ^2 values. The reduced chi-square χ^2 is given by the following equation [58]:

$$\chi^2 = \frac{\left(q_e^{\exp} - q_e^{\text{cal}}\right)^2}{q_e^{\text{cal}}} \tag{3}$$

where q_e^{cal} is the theoretical equilibrium adsorption capacity (mg g^{-1}) estimated from pseudo-first-order or pseudo-second-order kinetic equation, and $q_e^{\exp}$ is the experimental equilibrium adsorption capacity (mg g^{-1}) calculated by using Eq. (1).

The linearized form of pseudo-first-order kinetic model is given by the following equation [55–57]:

$$\ln\left(q_e - q_t\right) = \ln\left(q_e\right) - k_1 t \tag{4}$$

where q_t is the amount of the adsorbed dye at various times t (mg g^{-1}), q_e is the amount of the adsorbed dye at equilibrium

(mg g^{-1}), t is the contact time (h), and k_1 is the rate constant for pseudo-first-order reaction (h^{-1}). The values of k_1 and q_e^{cal} at the studied temperatures are calculated using the values of the slope and intercept of the linear fit plots of $\ln(q_e - q_t)$ vs. t, as shown in Fig. 3a. The calculated kinetic parameters along with the values of R^2, χ^2, and q_e^{exp} for MB and CV at the studied temperatures are presented in Table 1. The results show that the R^2 values obtained at the studied temperatures for the pseudo-first-order kinetic model were found to be in the range of 0.976–0.993 for MB and 0.871–0.954 for CV. In addition, results given in Table 1 demonstrate that there is a large difference between the values of theoretical q_e^{cal} and experimental q_e^{exp} equilibrium adsorption capacity obtained from this kinetic model at the studied temperatures, which is obviously reflected by the high χ^2 values determined for MB (6.90–33.2) and CV (17.3–44.3). These findings suggest that the pseudo-first-order kinetic model was not the suitable model to describe the adsorption processes of MB and CV on the monolith surface.

The pseudo-second-order kinetic model assumes that the adsorption process is controlled by chemical adsorption steps [52]. The linearized form of the pseudo-second-order kinetic model is given by the following equation [55–57]:

$$\frac{t}{q_t} = \frac{1}{k_2 q_e^2} + \frac{1}{q_e} t \tag{5}$$

where k_2 is the rate constant for pseudo-second-order reaction (g mg^{-1} h^{-1}). The values of k_2 and q_e^{cal} at the studied temperatures are calculated using the values of the slope and intercept of the linear fit plots of t/q_t vs. t, as shown in Fig. 3b. The calculated kinetic parameters along with the values of R^2, χ^2, and q_e^{exp} for MB and CV are listed in Table 1. As can be seen from Fig. 3b, the plots for MB and CV found to be linear with R^2 values equal to 1.0. The high R^2 values and very low χ^2 values obtained at the studied temperatures for the pseudo-second-order kinetic model makes it the suitable kinetic model to explain the experimental kinetic data of MB and CV adsorption onto the monolith. In addition, results show that the theoretical q_e^{cal} values evaluated from the pseudo-second-order kinetic equation were in good agreement with the experimental q_e^{exp} values for MB and CV at the studied temperatures. These findings confirm that the pseudo-second-order was the suitable kinetic model to explain the adsorption kinetics of MB and CV onto the synthesized monolith. Similar results have

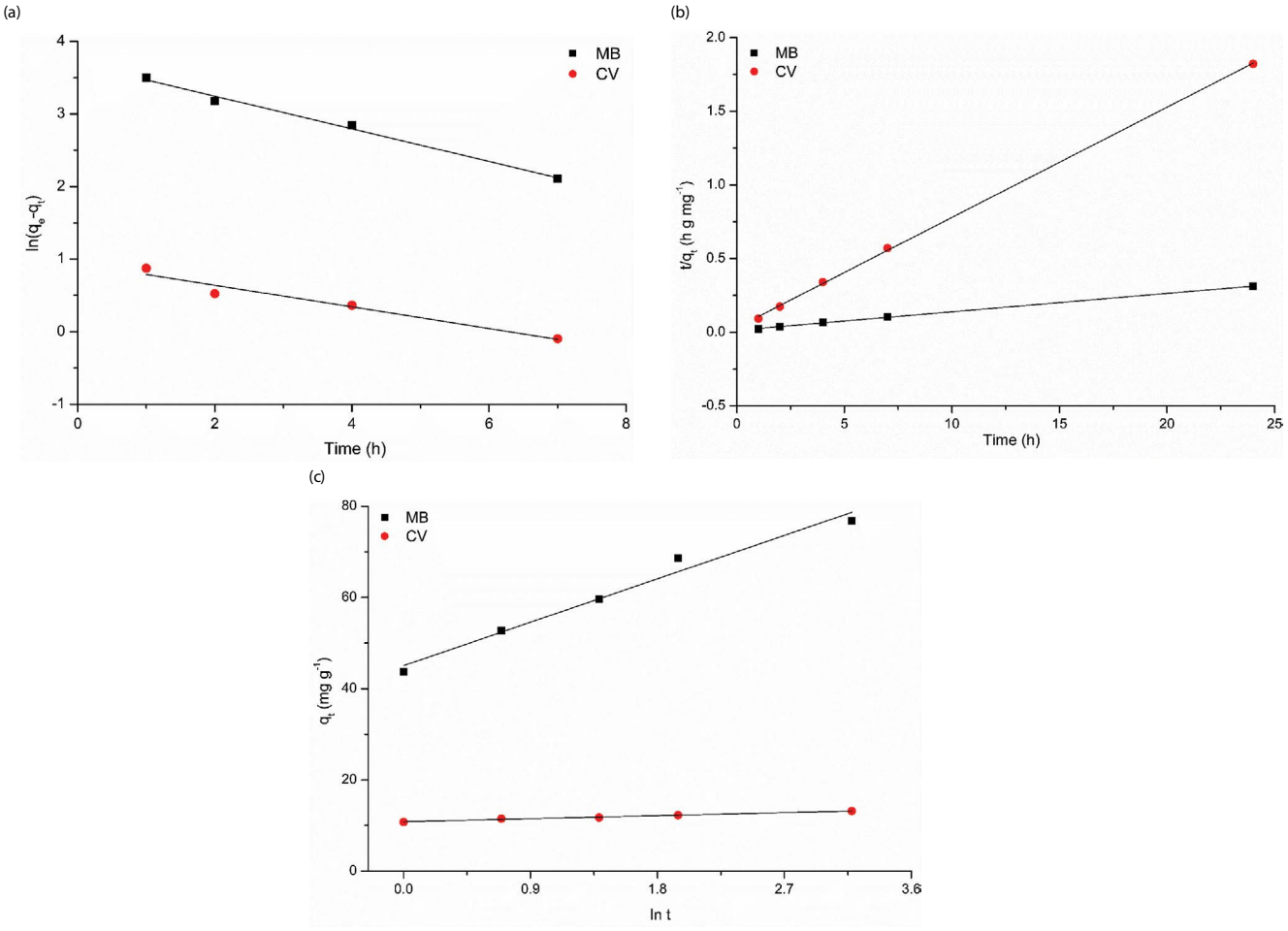

Fig. 3. (a) Pseudo-first-order, (b) pseudo-second-order, and (c) Elovich kinetic models for the adsorption of MB and CV onto the monolith at pH = 5.0 for MB and 4.0 for CV, temperature = 25°C, contact time = 1–24 h, and initial dye concentration = MB (50 mg L^{-1}) and CV (10 mg L^{-1}).

Table 1
Calculated parameters of pseudo-first-order, pseudo-second-order, and Elovich kinetic models for the adsorption of MB and CV dyes onto the synthesized monolith at pH = 5.0 for MB and 4.0 for CV, temperature = 25°C, 35°C, and 45°C, contact time = 1–24 h, and initial dye concentration = MB (50 mg L^{-1}) and CV (10 mg L^{-1})

Dye	MB			CV		
Temperature (°C)	25°C	35°C	45°C	25°C	35°C	45°C
q_e^{exp} (mg g^{-1})	76.80	71.48	66.62	13.18	13.88	14.10
Pseudo-first-order						
q_e^{cal} (mg g^{-1})	40.25	40.89	48.35	2.55	3.38	4.87
k_1 (h^{-1})	0.23	0.23	0.28	0.15	0.17	0.29
R^2	0.989	0.976	0.993	0.935	0.954	0.871
χ^2	33.2	22.9	6.90	44.3	32.6	17.3
Pseudo-second-order						
q_e^{cal} (mg g^{-1})	80.13	75.01	70.77	13.37	14.14	14.35
k_2 (g mg^{-1} h^{-1})	0.01	0.01	0.01	0.18	0.14	0.13
R^2	1.00	1.00	1.00	1.00	1.00	1.00
χ^2	0.138	0.166	0.243	0.003	0.005	0.006
Elovich						
α (mg g^{-1} h^{-1})	751.2	527.2	183.1	14.45	11.15	10.04
β (g mg^{-1})	0.095	0.098	0.085	1.36	1.03	0.924
R^2	0.972	0.953	0.923	0.985	0.995	0.896

been reported by authors working on the adsorption of MB and/or CV dyes onto porous carbon monolith [31–33], activated carbon [8,17,24], eggshells [21], and N-succinyl-chitosan-*g*-polyacrylamide/attapulgite composite [18].

The Elovich kinetic model has been successfully used to describe the adsorption of gases onto solid adsorbents [56]. Elovich kinetic model is given by the following equation [56]:

$$q_t = \frac{1}{\beta}\ln(\alpha\beta) + \frac{1}{\beta}\ln t \quad (6)$$

where q_t represents the initial adsorption rate (mg g^{-1} min^{-1}) and β is the desorption constant associated with the extent of the surface coverage and activation energy for chemisorption (mg g^{-1}). The values of α and β at the studied temperatures are calculated using the values of the slope (1/β) and intercept (1/β ln (αβ)) of the linear plots of q_t vs. ln*t*, as shown in Fig. 3c. The calculated kinetic parameters along with the values of R^2 for MB and CV are listed in Table 1. According to these results, the R^2 values obtained at the studied temperatures for the Elovich kinetic model were found to be in the range of 0.923–0.972 for MB and 0.896–0.995 for CV. These findings reveal that the experimental kinetic results obtained for MB and CV could be described by the Elovich kinetic model. The values of R^2 obtained for the pseudo-first-order, the pseudo-second-order, and the Elovich kinetic models are all high. However, the R^2 values for the pseudo-second-order kinetic model are equal to 1.0 and slightly higher than that of pseudo-first-order and Elovich kinetic models (Table 1). These results confirm that the pseudo-second-order kinetic model agrees well with the experimental data and can be successfully applied to explain the dyes adsorption onto the monolith surface.

3.3. Adsorption isotherms

3.3.1. Adsorption isotherm curves

It is reported that the shape of adsorption isotherm curves has a strong effect on the adsorption process performance as it provides important information to understand the nature of adsorption process [59,60]. Adsorption isotherm curves obtained for MB and CV at the studied temperatures are illustrated in Fig. 4. As can be seen from these isotherm curves, there is an increase in the adsorption capacity q_e for both dyes with increasing equilibrium concentration C_e, which might be explained by the increase in the initial dye concentration [44]. The increase in adsorption capacity with increase in initial dye concentration can be explained by the increase in the diffusion of the dye molecules from the bulk solution to the monolith pores present within the monolithic scaffold [61]. In addition, the increase in initial dye concentration results in an enhancement of the electrostatic interaction between the negatively charged sulfonate groups and cationic dye on the monolith surface, and thereby results in the increase of the adsorption capacity of the investigated dye [44].

The results given in Fig. 4 show that the isotherm curves obtained for MB do not reach a plateau region at all studied temperatures, which imply that the monolayer for MB was not completely formed on the monolith surface. For CV, these isotherm curves reach a plateau region at higher equilibrium concentration at 25°C and 35°C, which means that the monolayer for CV was formed on the monolith surface at this dye concentration. According to Giles and Smith, four main types of adsorption isotherms (L, H, S, and C) are classified based on the shape of adsorption isotherm curves [60]. As can be seen from Fig. 4a, the shape of the isotherm curves obtained for MB at the studied temperatures indicates L1-type adsorption isotherm. It is accepted that L1-type isotherms are usually used to describe the adsorption process of ionic adsorbates (e.g., ionic dyes and metal ions) [60]. Furthermore, L1-type isotherms assume that adsorption of MB on the monolith surface proceeds until a monolayer is completely formed, with the formation of multilayers on the monolith surface not being possible due to the electrostatic repulsion forces between the adsorbed dye molecules and those present in the bulk solution [60]. Fig. 4b indicates S2-type isotherm for CV at the studied temperatures according to Giles and Smith classifications [60]. In S2-type isotherms, adsorption of solute on the adsorbent follows cooperative adsorption mechanism, where the adsorbate molecules having the ability to bind at one binding site on the adsorbent surface (i.e., formation of multilayers), which could be affecting other binding sites on the same adsorbent [58]. In addition, the cooperative adsorption mechanism assumes that the adsorbate interaction at the surface of adsorbent is stronger

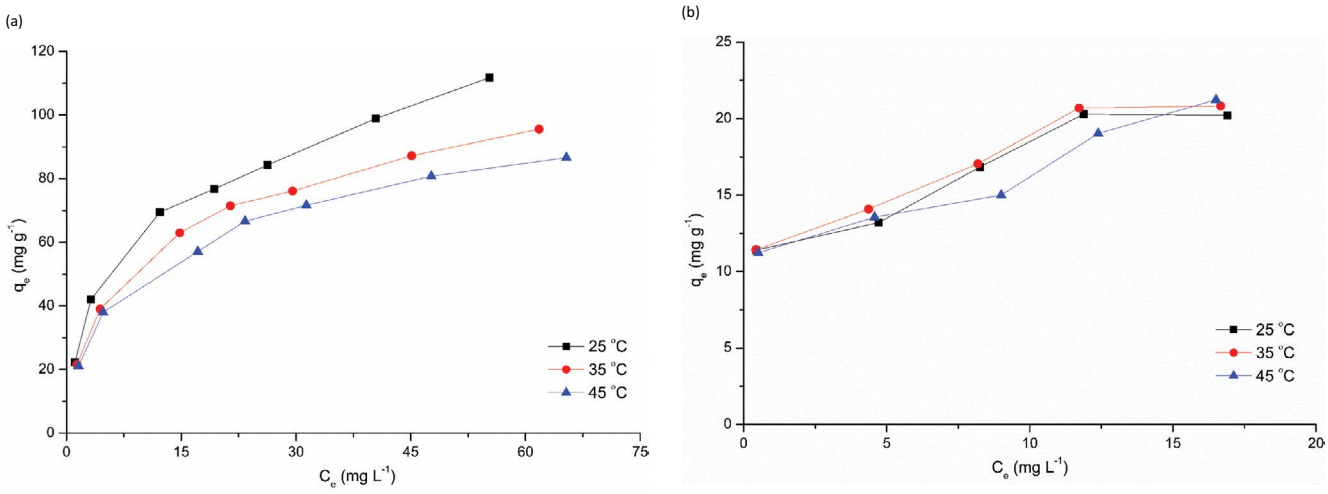

Fig. 4. Adsorption isotherm curves for (a) MB and (b) CV onto the monolith at temperature = 25°C, 35°C, and 45°C, contact time = 24 h, monolith dosage = 10 mg/25 mL, and initial dye concentration = MB (50 mg L^{-1}) and CV (10 mg L^{-1}).

than adsorbate interaction in the bulk solution, which in turn results in the formation of multilayers of adsorbate at the surface of adsorbent [59,60,63].

The results in Fig. 4 show that the adsorption capacity of MB and CV decreases with increasing temperature, indicating that adsorption of both dyes onto the monolith was an exothermic process. The decrease in the adsorption capacity of both dyes with increasing temperature might be explained by weakening of the electrostatic interactions between the negatively charged sulfonate groups and the positively charged dye molecules on the monolith surface.

3.3.2. Langmuir, Freundlich, Dubinin–Radushkevich, and Temkin isotherms

In the adsorption process, modelling of the experimental equilibrium data is an important work to predict the adsorption mechanism and to quantify the theoretical adsorption capacity of the adsorbent [58,62,64–67]. In the present work, we propose to fit the experimental equilibrium data obtained for MB and CV at the studied temperatures to the linearized equations of the Langmuir, Freundlich, Dubinin–Radushkevich, and Temkin adsorption isotherm models [58,62,65,66]. These fittings will allow to determine for each adsorption isotherm model the fitting parameters, and consequently, to find out the suitable isotherm model that can be used to describe the experimental equilibrium data.

The Langmuir isotherm model describes a monolayer formation of adsorbate on a homogeneous surface of adsorbent without any interaction between the adsorbed molecules [65,66]. This model assumes that all the binding sites on the adsorbent surface are identical and energetically equivalent and have the same adsorption capacity (i.e., homogenous sites) [62,66]. The linear form of the Langmuir isotherm model is expressed as [58,65]:

$$\frac{C_e}{q_e} = \frac{1}{q_e^{\max} K_L} + \frac{C_e}{q_e^{\max}} \tag{7}$$

where $q_e^{\max}$ is the maximum quantity of MB or CV adsorbed per unit mass of monolith at monolayer coverage (mg g^{-1}), K_L is the Langmuir constant related to the adsorption enthalpy and to the affinity of the adsorbent towards the adsorbate (L mg^{-1}). The values of K_L and $q_e^{\max}$ are calculated using the values of the slope ($1/q_e^{\max}$) and intercept ($1/q_e^{\max}K_L$) of the linear plot of C_e/q_e vs. C_e as shown in Figs. 5 and 6. The value of K_L is then used to calculate the value of the separation factor R_L according to the following equation [58,65]:

$$R_L = \frac{1}{1 + K_L C_0} \tag{8}$$

The R_L value is usually used to predict the favourability of the adsorption process. It is reported that R_L values indicate the adsorption process to be either favorable if $0 < R_L < 1$, unfavorable if $R_L > 1$, linear if $R_L = 1$, and irreversible if $R_L = 0$ [44,58,65].

The Freundlich isotherm is an empirical model used to describe multilayers formation of adsorbate on a heterogeneous surface of adsorbate. The linear form of the Freundlich isotherm is expressed as [58,65,66]:

$$\log q_e = \log K_F + \frac{1}{n} \log C_e \tag{9}$$

where K_F ((mg g^{-1})(L $mg^{-1})^{1/n}$) is the Freundlich constant represents the degree of adsorption and n is an empirical constant that is related to the intensity of the adsorption process. The magnitude of adsorption intensity (n) measures the degree of deviation from the linearity of adsorption (i.e., surface heterogeneity). It is accepted that the adsorption is classified as linear if $n = 1$, physical if $n > 1$, and chemical adsorption if $n < 1$ [58,63]. On the other hand, the adsorption is classified as normal equilibrium if $1/n < 1$ and as cooperative adsorption if $1/n > 1$ [24]. The values of adsorption capacity (K_F) and the adsorption intensity (n) can be easily calculated using the values of the slope ($1/n$) and intercept ($\log K_F$) of the linear plot of $\log q_e$ vs. $\log C_e$ as shown in Figs. 5 and 6.

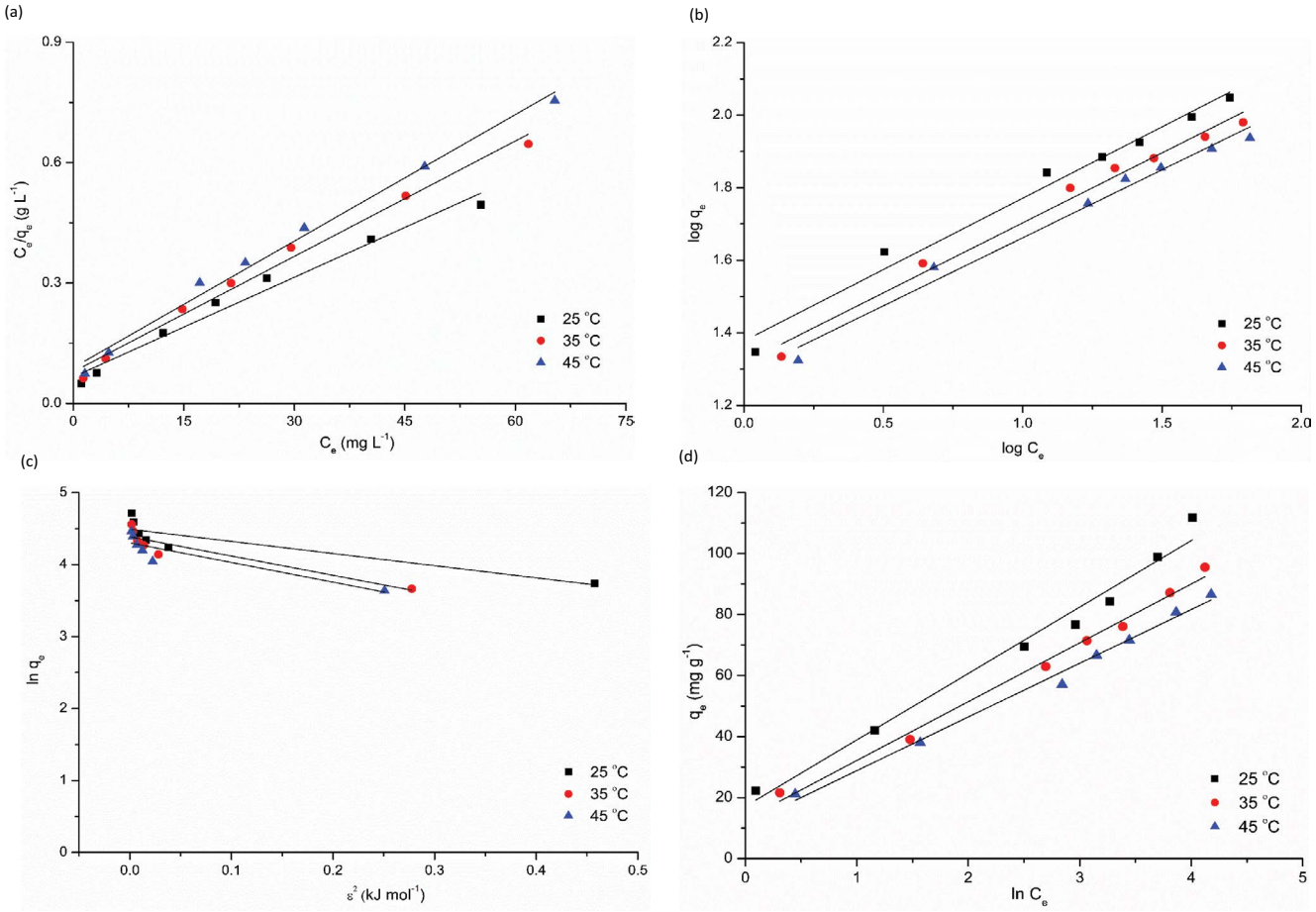

Fig. 5. Plots of linearized adsorption isotherm of MB onto the monolith: (a) Langmuir model, (b) Freundlich model, (c) Dubinin–Radushkevich model, and (d) Temkin model at pH = 5.0, temperature = 25°C, 35°C, and 45°C, contact time = 24 h, monolith dosage = 10 mg/25 mL, MB concentration range = (10–100 mg L^{-1}).

The Dubinin–Radushkevich isotherm model was used to distinguish between chemical and physical adsorption [58]. This model is usually used to calculate the binding energy of adsorption E (kJ mol^{-1}) that describes the transfer of one mole of adsorbate from bulk solution to the adsorbent surface. The value of E was usually used to characterize the type of the adsorption as physical adsorption if E < 8 kJ mol^{-1} or chemical adsorption if E > 8 kJ mol^{-1}. The liner form of the Dubinin–Radushkevich isotherm model is given by the following equation [58]:

$$\ln\left(q_e\right) = \ln\left(q_e^{\max}\right) - \beta\varepsilon^2 \tag{10}$$

$$\varepsilon = RT\ln\left(1+\frac{1}{C_e}\right) \tag{11}$$

where R is the gas constant (J K^{-1} mol^{-1}), T is the temperature (K), ε is the Polanyi potential, β is the activity coefficient that relates to mean adsorption energy (mol^2 kJ^{-2}). E (kJ mol^{-1}) can be calculated using the following equation:

$$E = \frac{1}{\sqrt{2\beta}} \tag{12}$$

The Temkin isotherm model describes the interaction between adsorbate and adsorbent as a chemical adsorption process. This model is based on the assumption that the adsorbent has homogenous binding energy sites and the heat of adsorption of all adsorbate molecules decreases linearly with increasing surface coverage [58]. The linear form of the Temkin isotherm model is expressed as [58]:

$$q_e = \frac{RT}{b}\ln A_T + \frac{RT}{b}\ln C_e \tag{13}$$

$$B_T = \frac{RT}{b} \tag{14}$$

where A_T is the Temkin isotherm equilibrium binding constant (L g^{-1}), b is the Temkin isotherm constant (mg L^{-1}), B_T is the constant related to the heat of adsorption (J mol^{-1}), and T is the absolute temperature (K). The values of A_T, b, and B_T can be calculated using the values of the slope (B) and intercept ($B_T \ln A_T$) of the linear plot of q_e vs. $\ln C_e$ as shown in Figs. 5 and 6.

The plots of the Langmuir, Freundlich, Dubinin–Radushkevich, and Temkin isotherm models for adsorption of MB and CV onto the monolith at the studied temperatures

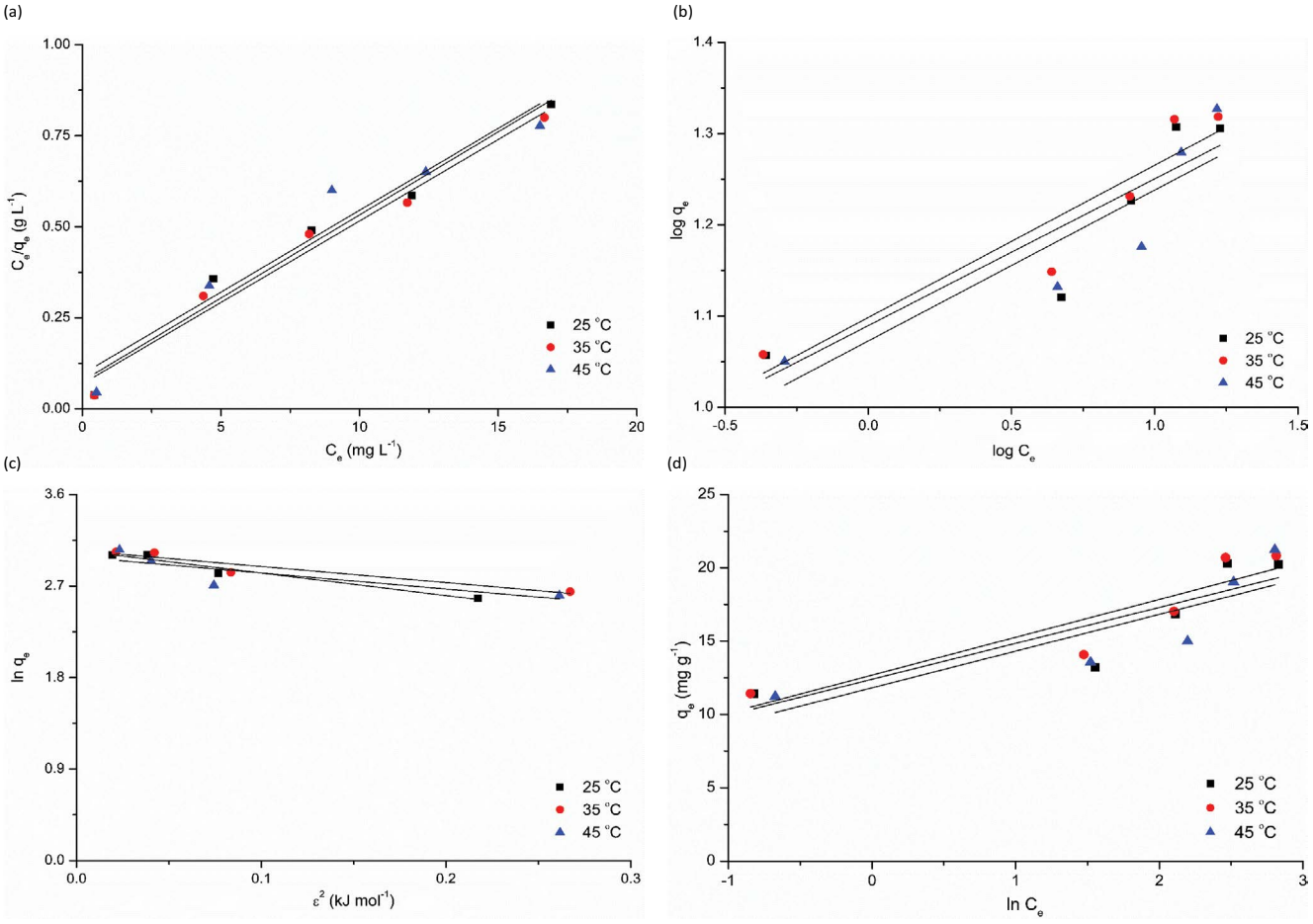

Fig. 6. Plots of linearized adsorption isotherm of CV onto the monolith: (a) Langmuir model, (b) Freundlich model, (c) Dubinin–Radushkevich model, and (d) Temkin model at pH = 4.0, temperature = 25°C, 35°C, and 45°C, contact time = 24 h, monolith dosage = 10 mg/25 mL, MB concentration range = (5–25 mg L^{-1}).

are shown in Figs. 5 and 6. In addition, Table 2 summarizes the isotherm fitting parameters calculated from these isotherm models together with q_e^{exp}, R^2, and χ^2 values. The different adsorption data obtained for MB and CV (Table 2) could be explained in terms of molecular size, geometry, and molecular weight of these dyes. As can be seen from the chemical structures of MB and CV dyes given in Fig. 1, CV has trigonal planar structure consists of large and bulky triphenylmethane group ($(C_6H_5)_3CH$), whereas MB has a linear structure consists of small size thiazine and azine groups [64]. These findings imply that CV has a larger molecular size compared to MB. As a general trend, dye molecules with smaller molecular size exhibit higher mobility and faster diffusion into the adsorbent pores when compared to larger dye molecules, and thereby results in a high removal efficiency [22,68,69].

Linear plots for the Langmuir, Freundlich, and Temkin isotherms for adsorption of MB onto the monolith show excellent fit to the experimental equilibrium data with high R^2 values (>0.98). This confirms that these isotherm models can adequately describe the adsorption of MB onto the synthesized monolith due to the presence of homogeneous and heterogeneous binding sites. Furthermore the results given in Table 2 show that the R^2 values obtained for the Dubinin–Radushkevich isotherm model were found to be in the range of 0.75-0.81 for MB (Table 2).

Among all the studied isotherm models, results in Table 2 demonstrate that the Langmuir isotherm was the only isotherm model that describes the adsorption of CV onto the monolith with high R^2 values (>0.92) [70]. This implies that the Langmuir isotherm model can adequately describe the adsorption process of CV onto the synthesized monolith by the formation of monolayer coverage at the monolith surface. Another observation shown in Table 2 is that the theoretical q_e^{max} values evaluated from the Langmuir isotherm model were in good agreement with the experimental q_e^{exp} values for MB and CV at the studied temperatures, which is obviously reflected by the very low χ^2 values determined for MB (0.64–0.89) and CV (0.05–0.13) (Table 2). These findings confirm also that the Langmuir isotherm model was the most suitable model to explain the adsorption of MB and CV onto the synthesized monolith. In literature, similar findings were reported for the adsorption isotherms of various pollutant-adsorbent systems [71,72].

Results in Table 2 show that the R_L values evaluated from the Langmuir isotherm model were ranged between

Table 2
Isotherm parameters obtained for Langmuir, Freundlich, Dubinin–Radushkevich, and Temkin isotherm models calculated for the adsorption of MB and CV dyes at temperature = 25°C, 35°C, and 45°C, contact time = 24 h, monolith dosage = 10 mg/25 mL

Dye	MB			CV		
Temperature (°C)	25°C	35°C	45°C	25°C	35°C	45°C
q_e^{exp} (mg g^{-1})	111.7	95.6	86.6	20.22	20.83	21.23
Langmuir isotherm						
q_e^{max} (mg g^{-1})	120.5	105.3	95.2	21.93	22.37	22.24
K_L (L mg^{-1})	0.13	0.12	0.12	0.60	0.65	0.47
R_L	0.07	0.08	0.08	0.06	0.06	0.08
R^2	0.98	0.99	0.99	0.96	0.97	0.92
χ^2	0.64	0.89	0.78	0.13	0.11	0.05
Freundlich isotherm						
K_F ((mg g^{-1}) (L mg^{-1})$^{1/n}$)	23.9	20.8	19.4	12.3	12.5	11.8
n	2.54	2.59	2.67	6.21	6.00	6.10
R^2	0.98	0.98	0.98	0.76	0.85	0.74
Dubinin–Radushkevich isotherm						
q_e^{max} (mg g^{-1})	89.3	80.4	73.9	21.1	21.1	19.8
β (mol^2 kJ^{-2})	1.69	2.68	2.73	2.22	1.58	1.58
E (kJ mol^{-1})	0.54	0.43	0.43	0.47	0.56	0.56
R^2	0.75	0.81	0.77	0.94	0.86	0.55
χ^2	5.623	2.850	2.186	0.040	0.004	0.100
Temkin isotherm						
B_T (J mol^{-1})	21.8	19.3	17.6	2.45	2.58	2.50
A_T (L g^{-1})	2.20	1.95	1.89	158	136	112
b (mg L^{-1})	114	133	150	1012	993	1056
R^2	0.98	0.99	0.99	0.69	0.78	0.65

0 and 1 ($0 < R_L < 1$), indicating the favorable adsorption of MB and CV by the formation of homogenous monolayer coverage of dye molecules at the monolith surface. The maximum monolayer adsorption capacities for MB and CV onto the synthesized monolith were found to be 121 and 22 mg g^{-1}, respectively (Table 2). The maximum adsorption equilibrium capacity values of MB and CV on the synthesized polyacrylamide-based monolith have been compared with those of various adsorbents reported in the literature (Table 3). The comparison shows that the synthesized monolith has a comparable adsorption capacity of MB and CV to some of these reported adsorbents. In addition, data in Table 3 demonstrate that the synthesized monolith exhibited a slightly lower adsorption capacity of MB and CV than some of these reported adsorbents, which might be attributed to the differences in the experimental conditions and type of adsorbent.

The results obtained show that the values of heterogeneity factor (n) obtained for MB and CV were found to be greater than 1.0, which confirm the favorable physical adsorption of these dyes onto the monolith surface [40,44]. Furthermore, the large values of n obtained for CV (ca. 6.21) compared to MB (ca. 2.54) suggest strong interaction between the cationic CV molecules and the negatively charged sulfonate groups present on the monolith surface [21]. We also observed that the K_F values determined for MB decrease with increasing temperature, whereas for CV, there is slight decrease in the K_F values with increasing temperature. For example, K_F for MB decreases from about 23.9 ((mg g^{-1})(L mg^{-1})$^{1/n}$) at 25°C to about 20.8 ((mg g^{-1}) (L mg^{-1})$^{1/n}$) at 35°C and decreases further to about 19.4 ((mg g^{-1})(L mg^{-1})$^{1/n}$) at 45°C (Table 2). These findings confirm that the adsorption process of MB onto the monolith surface is an exothermic. Furthermore, it was observed that the K_F values for MB are higher than those for CV, which might be attributed to its small molecular size compared to CV.

The fitting isotherm parameters obtained from the Langmuir, Freundlich, and Temkin isotherm models suggest normal equilibrium physical adsorption mechanism for the investigated dyes as the values of $1/n$ for these dyes are less than 1.0. According to this mechanism, monolayer coverage of the dye molecules is formed onto the monolith surface by the physical electrostatic interactions between the cationic dye molecules and the negatively charged sulfonate groups present on the monolith surface. Then, the formed monolayer forms multilayers by chemical interaction with the dye molecules present in the bulk solution [40,44,63]. The results given in Table 2 show that the values of the binding energy (E) obtained from the Dubinin–Radushkevich model for MB and CV dyes were less than 8 kJ mol^{-1} at the studied temperatures and thus the adsorption mechanism involved is physical adsorption [40,44]. It is reported that physical adsorption process takes place with bond energies less than 8 kJ mol^{-1}, while adsorption process takes place by chemical ion-exchange mechanism with bond energies between 8 to 16 kJ mol^{-1} [21]. According to the results listed in Table 2, there is a decrease in the B_T values for MB with increasing temperature, indicating that the adsorption of MB onto the monolith is an exothermic process. For example, B_T for MB decreases from about 21.8 J mol^{-1} at 25°C to about 19.3 J mol^{-1} at 35°C and decreases further to about 17.6 J mol^{-1} at 45°C (Table 2). Additionally, it was observed that there is no change in the B_T values for CV with increasing temperature (Table 2). Results in Table 2 show that the values obtained from the Temkin isotherm model were A_T = 2.2 L g^{-1} and B_T = 0.022 kJ mol^{-1} for MB and A_T = 158 L g^{-1} and B_T = 0.002 kJ mol^{-1} for CV at 25°C, which indicates that the adsorption of these dyes onto the synthesized monolith occurred via physisorption (Table 2).

3.4. Thermodynamic studies

In order to study the spontaneity of MB and CV adsorption onto the synthesized monolith, different thermodynamic parameters such as standard Gibbs free energy change $\Delta G°$ (kJ mol^{-1}), standard entropy change $\Delta S°$ (J K^{-1} mol^{-1}), and standard enthalpy change $\Delta H°$ (kJ mol^{-1}) were evaluated for these dyes. In the present study, $\Delta H°$ and $\Delta S°$ were calculated using the Van't Hoff equation as follows [40,44]:

Table 3
Comparative account of the adsorption capacity of MB and CV dyes by different adsorbents

Adsorbent	q_{max} MB (mg g^{-1})	q_{max} CV (mg g^{-1})	Conditions	Reference
Porous carbon monoliths	127	–	T = 25°C; pH = 7.5; time = 16 h	[33]
Fennel seed	13.4	18.2	pH (CV) = 4.0; pH (MB) = 6.0; T = 25°C; time = 1.5 h	[30]
Zirconium oxide/activated carbon composite	208	204	pH (CV) = 4.0; pH (MB) = 6.0; T = 25°C; time = 10 min	[23]
Cellulose/activated carbon composite monolith	158	–	pH = 7.0; T = 25°C; time = 30 h	[31]
Surfactant modified carbon coated monolith	388	–	pH = 10; T = 25°C; time = 48 h	[32]
N-succinyl-chitosan-*g*-polyacrylamide/attapulgite composite	135	–	pH (CV) = 4.0; T = 25°C; time = 24 h	[18]
A natural clay mineral	77	330	pH (CV) = 7.5; pH (MB) = 7.0; T = 30°C; time = 3.0 h	[13]
Palm kernel shell-derived biochar	–	24	pH = 7.0; T = 25°C; time = 24 h	[14]
Agro-waste-derived activated carbon	14	7.6	pH = 7.0; T = 25°C; time = 3.0 h	[68]
Polyacrylamide-based monolith	121	22	pH (CV) = 4.0; pH (MB) = 5.0; T = 25°C; time = 24 h	This study

Table 4
Calculated thermodynamic parameters ($\Delta G°$, $\Delta H°$, and $\Delta S°$) at 298.15 K for the adsorption of MB and CV dyes onto the synthesized monolith

Dye	$\Delta G°$ (kJ mol^{-1})	$\Delta H°$ (kJ mol^{-1})	$\Delta S°$ (J K^{-1} mol^{-1})
MB	–3.18	–3.06	0.39
CV	–4.21	–3.82	1.30

$$\ln K_d = \frac{\Delta S°}{R} - \frac{\Delta H°}{RT} \tag{15}$$

$$K_d = \frac{q_e}{C_e} \tag{16}$$

where K_d is the distribution coefficient of MB or CV between the bulk aqueous phase and the solid monolith (L g^{-1}). The values of $\Delta H°$ and $\Delta S°$ are calculated using the values of the slope and intercept of the linear plot of $\ln K_d$ vs. $1/T$ as shown in Fig. 7. The values of $\Delta G°$ is calculated using the following equation:

$$\Delta G° = \Delta H° - T\Delta S° \tag{17}$$

The results of thermodynamic parameters determined for MB and CV are listed in Table 4. The negative values of $\Delta H°$ for MB (–3.06 kJ mol^{-1}) and CV (–3.82 kJ mol^{-1}) confirm the exothermic nature of the adsorption processes of these dyes onto the synthesized monolith. In addition, the negative $\Delta G°$ values indicate that adsorption of MB and CV dyes was spontaneous. The positive values of $\Delta S°$ for MB (+0.39 J K^{-1} mol^{-1}) and CV (+1.30 J K^{-1} mol^{-1}) show the affinity of the monolith toward MB and CV indicate that the two adsorption processes have an increased randomness at the solid–liquid interface [43].

3.5. Reusability of the monolith

The reusability of the synthesized monolith is an essential step and of great importance in wastewater treatment. With the aim to evaluate the reusability of the synthesized monolith, adsorption experiments were performed by mixing 25 mL of 50 mg L^{-1} MB solution with 0.01 g of the fresh monolith at 25°C and pH 5.0. The dye solution with the monolith was shaken for 24 h at 200 rpm. After reaching equilibrium, the suspension was filtered and the concentration of unabsorbed MB left in solution was determined by vis spectrophotometer. After that, the MB-loaded monolith was thoroughly washed with deionized water to remove any unabsorbed MB molecules. The regeneration process (desorption) was performed by mixing the MB-loaded monolith with 100 mL of 0.1 M HCl solution. The mixture was shaken for about 1 h at 200 rpm and filtered. Finally, the regenerated monolith was washed with deionized water and then dried to constant weight. All adsorption and desorption experiments were performed in triplicate. The next step is the reusability of the regenerated monolith that was investigated by performing adsorption experiment using it under the same experimental conditions as for the fresh monolith, and then compares the results for both. The percent removal of MB obtained for the regenerated and fresh monoliths were calculated and the results are illustrated in Fig. 8. For the fresh monolith, it was found that the percent removal is around 61.4%, while for the regenerated monolith it is around 61.3%. These results confirm that the synthesized monolith can be successfully employed for MB removal after regeneration without significant loss in the removal efficiency.

4. Conclusions

In the present work, a macroporous polyacrylamide-based monolith bearing negatively charged sulfonate

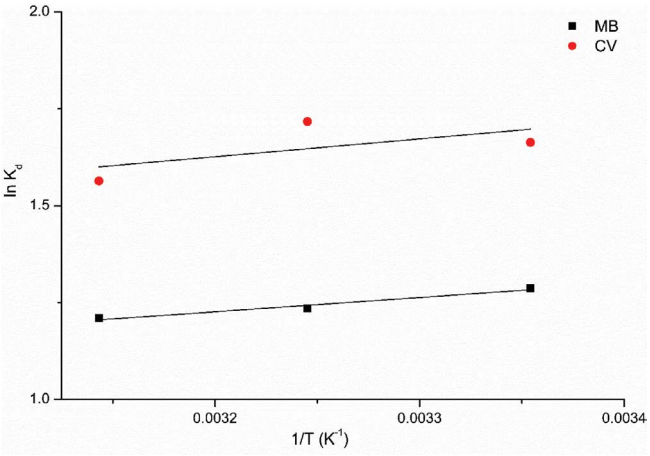

Fig. 7. Plots of lnK_d vs. 1/T for MB and CV at temperature = (25°C, 35°C, and 45°C), contact time = 24 h, monolith dosage = 10 mg/25 mL.

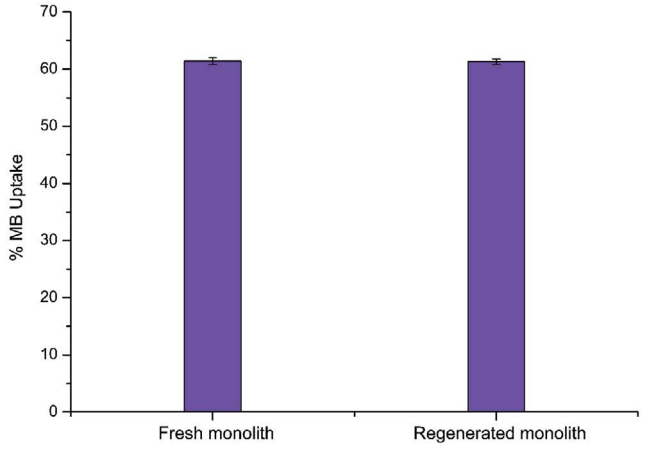

Fig. 8. Comparison between the values of percent removal obtained for MB on the fresh and regenerated monoliths. Temperature = 25°C, pH = 5.0, contact time = 24 h, MB concentration = 50 mg L^{-1}

groups was synthesized and tested as adsorbent for the efficient removal of MB and CV dyes from aqueous solutions using batch adsorption method. The results presented in this study demonstrate that the adsorption efficiency of the synthesized monolith is strongly affected by the experimental conditions such as solution pH, contact time, monolith dosage, and initial dye concentration. The adsorption kinetics for MB and CV followed pseudo-second-order kinetic model indicating that the adsorption is controlled by chemisorption rate determining step. The results show that the adsorption of MB and CV onto the synthesized monolith was better described by Langmuir isotherm model with the maximum monolayer adsorption capacity of 120.5 mg g^{-1} for MB and 21.93 mg g^{-1} for CV. The observed differences in adsorption data obtained for MB and CV dyes can be attributed to differences in the molecular size of these dyes. The calculated thermodynamic parameters showed that the adsorption of MB and CV onto the synthesized monolith exothermic and spontaneous. Reusability studies showed that the synthesized monolith could be successfully employed for MB removal after regeneration. According to the results obtained in this study, it can be concluded that the synthesized monolith can be used as an adsorbent for the effective removal of toxic dyes from wastewater.

Acknowledgements

Authors thank The University of Jordan, dean ship of scientific research (Amman, Jordan) and Al al-Bayt University (Mafraq, Jordan) for providing financial support and laboratory facilities to perform this work.

Conflicts of interest/Competing interests

The authors declare that they have no conflict of interest.

References

[1] S.P. Dubey, A.D. Dwivedi, M. Sillanpää, H. Lee, Y.-N. Kwon, C. Lee, Adsorption of As(V) by boehmite and alumina of different morphologies prepared under hydrothermal conditions, Chemosphere, 169 (2017) 99–106.
[2] N.B. Singh, G. Nagpal, S. Agrawal, Rachna, Water purification by using adsorbents: a review, Environ. Technol. Innovation, 11 (2018)187–240.
[3] Y. Li, S. Wang, Z. Shen, X. Li, Q. Zhou, Y. Sun, T. Wang, Y. Liu, Q. Gao, Gradient adsorption of methylene blue and crystal violet onto compound microporous silica from aqueous medium, ACS Omega, 5 (2020) 28382–28392.
[4] F. Mashkoor, A. Nasar, Magsorbents: potential candidates in wastewater treatment technology – a review on the removal of methylene blue dye, J. Magn. Magn. Mater., 500 (2020) 166408, doi: 10.1016/j.jmmm.2020.166408.
[5] M.T. Yagub, T.K. Sen, S. Afroze, H.M. Ang, Dye and its removal from aqueous solution by adsorption: a review, Adv. Colloid Interface Sci., 209 (2014) 172–184.
[6] M. Rafatullah, O. Sulaiman, R. Hashim, A. Ahmad, Adsorption of methylene blue on low-cost adsorbents: a review, J. Hazard. Mater., 177 (2010) 70–80.
[7] F. Chi, B. Song, B. Yang, Y. Lv, S. Ran, Q. Huo, Activation of peroxymonosulfate by $BiFeO_3$ microspheres under visible light irradiation for decomposition of organic pollutants, RSC Adv., 5 (2015) 67412–67417.
[8] Y. Kuang, X. Zhang, S. Zhou, Adsorption of methylene blue in water onto activated carbon by surfactant modification, Water, 12 (2020) 587, doi: 10.3390/w12020587.
[9] S. Liu, H. Ge, C. Wang, C. Wang, Y. Zou, J. Liu, Agricultural waste/graphene oxide 3D bio-adsorbent for highly efficient removal of methylene blue from water pollution, Sci. Total Environ., 628–629 (2018) 959–968.
[10] T.M.V. Ngo, T.H. Truong, T.H.L. Nguyen, T.T.A. Duong, T.H. Vu, T.T.T. Nguyen, T.D. Pham, Surface modified laterite soil with an anionic surfactant for the removal of a cationic dye (crystal violet) from an aqueous solution, Water Air Soil Pollut., 231 (2020) 285, doi: 10.1007/s11270-020-04647-2.
[11] W. Wei, L. Yang, W.H. Zhong, S.Y. Li, J. Cui, Z.G. Wei, Fast removal of methylene blue from aqueous solution by adsorption onto poorly crystalline hydroxyapatite nanoparticles, Dig. J. Nanomater. Biostruct., 10 (2015) 1343–1363.
[12] P. Zhang, D. O'Connor, Y. Wang, L. Jiang, T. Xia, L. Wang, D.C.W. Tsang, Y.S. Ok, D. Hou, A green biochar/iron oxide composite for methylene blue removal, J. Hazard. Mater., 384 (2020) 121286, doi: 10.1016/j.jhazmat.2019.121286.
[13] O.S. Omer, M.A. Hussein, B.H.M. Hussein, A. Mgaidi, Adsorption thermodynamics of cationic dyes (methylene blue and crystal violet) to a natural clay mineral from aqueous solution between 293.15 and 323.15 K, Arabian J. Chem., 11 (2018) 615–623.

[14] P.P. Kyi, J.O. Quansah, C.G. Lee, J.-K. Moon, S.-J. Park, The removal of crystal violet from textile wastewater using palm kernel shell-derived biochar, Appl. Sci., 10 (2020) 2251, doi: 10.3390/app10072251.
[15] Z.U. Zango, S.S. Imam, Evaluation of microcrystalline cellulose from groundnut shell for the removal of crystal violet and methylene blue, Nanosci. Nanotechnol., 8 (2018) 1–6.
[16] M. Sarabadan, H. Bashiri, S.M. Mousavi, Removal of crystal violet dye by an efficient and low cost adsorbent: modeling, kinetic, equilibrium and thermodynamic studies, Korean J. Chem. Eng., 36 (2019) 1575–1586.
[17] D. Pathania, S. Sharma, P. Singh, Removal of methylene blue by adsorption onto activated carbon developed from *Ficus carica* bast, Arabian J. Chem., 10 (2017) S1445–S1451.
[18] Q. Li, Y. Zhao, L. Wang, W. Aiqin, Adsorption characteristics of methylene blue onto the N-succinyl-chitosan-g-polyacrylamide/attapulgite composite, Korean J. Chem. Eng., 28 (2011) 1658–1664.
[19] D. Ghosh, K.G. Bhattacharyya, Adsorption of methylene blue on kaolinite, Appl. Clay Sci., 20 (2002) 295–300.
[20] I. Anastopoulos, A. Bhatnagar, B.H. Hameed, Y.S. Ok, M. Omirou, A review on waste-derived adsorbents from sugar industry for pollutant removal in water and wastewater, J. Mol. Liq., 240 (2017) 179–188.
[21] S. Chowdhury, S. Chakraborty, P.D. Saha, Removal of crystal violet from aqueous solution by adsorption onto eggshells: equilibrium, kinetics, thermodynamics and artificial neural network modeling, Waste Biomass Valorization, 4 (2013) 655–664.
[22] A.R. Abbasi, M. Karimi, K. Daasbjerg, Efficient removal of crystal violet and methylene blue from wastewater by ultrasound nanoparticles Cu-MOF in comparison with mechanosynthesis method, Ultrason. Sonochem., 37 (2017) 182–191.
[23] H.A. Ahsaine, Z. Anfar, M. Zbair, M. Ezahri, N. El Alem, Adsorptive removal of methylene blue and crystal violet onto micro-mesoporous Zr_3O/activated carbon composite: a joint experimental and statistical modeling considerations, J. Chem., 2018 (2018) 1–14, doi: 10.1155/2018/6982014.
[24] T. Aysu, M.M. Küçük, Removal of crystal violet and methylene blue from aqueous solutions by activated carbon prepared from *Ferula orientalis*, Int. J. Environ. Sci. Technol., 12 (2015) 2273–2284.
[25] S. Al-Shahrani, Phenomena of removal of crystal violet from wastewater using Khulays natural bentonite, J. Chem., 1 (2020), doi: 10.1155/2020/4607657.
[26] K. Mohanty, J.T. Naidu, B.C. Meikap, M.N. Biswas, Removal of crystal violet from wastewater by activated carbons prepared from rice husk, Ind. Eng. Chem. Res., 45 (2006) 5165–5171.
[27] L.S. Maia, A.I.C. da Silva, E.S. Carneiro, F.M. Monticelli, F.R. Pinhati, D.R. Mulinari, Activated carbon from palm fibres used as an adsorbent for methylene blue removal, J. Polym. Environ., 29 (2021) 1162–1175.
[28] A. Adak, M. Bandyopadhyay, A. Pal, Removal of crystal violet dye from wastewater by surfactant-modified alumina, Sep. Purif. Technol., 44 (2005) 139–144.
[29] A. Awadallah-F, S.A. Al-Muhtaseb, Removal of crystal violet from wastewater using resorcinol-formaldehyde carbon xerogels, Sep. Sci. Technol., 51 (2016) 403–415.
[30] T.K. Hussein, N.A. Jasim, Removal of crystal violet and methylene blue from synthetic industrial wastewater using fennel seed as an adsorbent, J. Eng. Sci.Technol., 14 (2019) 2947–2963.
[31] Q. Bai, Q. Xiong, C. Li, Y. Shen, H. Uyama, Hierarchical porous cellulose/activated carbon composite monolith for efficient adsorption of dyes, Cellulose, 24 (2017) 4275–4289.
[32] M.R. Malekbala, M.A. Khan, S. Hosseini, L.C. Abdullah, T.S.Y. Choong, Adsorption/desorption of cationic dye on surfactant modified mesoporous carbon coated monolith: equilibrium, kinetic and thermodynamic studies, J. Ind. Eng. Chem., 21 (2015) 369–377.
[33] X. He, K.B. Male, P.N. Nesterenko, D. Brabazon, B. Paull, J.H.T. Luong, Adsorption and desorption of methylene blue on porous carbon monoliths and nanocrystalline cellulose, ACS Appl. Mater. Interfaces, 5 (2013) 8796–8804.
[34] M. Sharma, S. Hazra, S. Basu, Kinetic and isotherm studies on adsorption of toxic pollutants using porous ZnO@SiO_2 monolith, J. Colloid Interface Sci., 504 (2017) 669–679.
[35] S.A. El-Safty, A. Shahat, M.R. Awual, Efficient adsorbents of nanoporous aluminosilicate monoliths for organic dyes from aqueous solution, J. Colloid Interface Sci., 359 (2011) 9–18.
[36] E. Ayranci, O. Duman, In-situ UV-Visible spectroscopic study on the adsorption of some dyes onto activated carbon cloth, Sep. Sci. Technol., 44 (2009) 3735–3752.
[37] O. Duman, S. Tunç, T.G. Polat, Adsorptive removal of triarylmethane dye (Basic red 9) from aqueous solution by sepiolite as effective and low-cost adsorbent, Microporous Mesoporous Mater., 210 (2015) 176–184.
[38] O. Duman, S. Tunç, T.G. Polat, B.K. Bozoğlan, Synthesis of magnetic oxidized multiwalled carbon nanotube-κ-carrageenan-Fe_3O_4 nanocomposite adsorbent and its application in cationic methylene blue dye adsorption, Carbohydr. Polym., 147 (2016) 79–88.
[39] O. Duman, T.G. Polat, C.Ö. Diker, S. Tunç, Agar/κ-carrageenan composite hydrogel adsorbent for the removal of methylene blue from water, Int. J. Biol. Macromol., 160 (2020) 823–835.
[40] A.A. Al-Massaedh, F.I. Khalili, Removal of thorium(IV) ions from aqueous solution by polyacrylamide-based monoliths: equilibrium, kinetic and thermodynamic studies, J. Radioanal. Nucl. Chem., 327 (2021) 1201–1217.
[41] S. Xie, F. Svec, J.M.J. Fréchet, Porous polymer monoliths: preparation of sorbent materials with high-surface areas and controlled surface chemistry for high-throughput, online, solid-phase extraction of polar organic compounds, Chem. Mater., 10 (1998) 4072–4078.
[42] G. Guiochon, Monolithic columns in high-performance liquid chromatography, J. Chromatogr. A, 1168 (2007) 101–168.
[43] Y. Hu, S. Giret, R. Meinusch, J. Han, F-G. Fontaine, F. Kleitz, D. Dominic Lariviere, Selective separation and preconcentration of Th(IV) using organo-functionalized, hierarchically porous silica monoliths, J. Mater. Chem. A, 7 (2019) 289–302.
[44] A.A. Al-Massaedh, F.I. Khalili, Removal of heavy metal ions from aqueous solution by anionic polyacrylamide-based monolith: equilibrium, kinetic and thermodynamic studies, Desal. Water Treat., 228 (2021) 297–311.
[45] M. Sharma, J. Singh, S. Hazra, S. Basu, Remediation of heavy metal ions using hierarchically porous carbon monolith synthesized via nanocasting method, J. Environ. Chem. Eng., 6 (2018) 2829–2836.
[46] A.A. Al-Massaedh, U. Pyell, Mixed-mode acrylamide-based continuous beds bearing tert-butyl groups for capillary electrochromatography synthesized via complexation of N-tert-butylacrylamide with a water-soluble cyclodextrin. Part I: retention properties, J. Chromatogr. A, 1477 (2016) 114–126.
[47] L. Uzun, D. Türkmen, E. Yilmaz, S. Bektas, A. Denizli, Cysteine functionalized poly(hydroxyethyl methacrylate) monolith for heavy metal removal, Colloids Surf., A, 330 (2008) 161–167.
[48] I. Nischang, T.J. Causon, Porous polymer monoliths: from their fundamental structure to analytical engineering applications, TrAC, Trends Anal. Chem., 75 (2016) 108–117.
[49] R.J. Groarke, D. Brabazon, Methacrylate polymer monoliths for separation applications, Materials, 9 (2016) 446–479.
[50] S. Wang, R. Zhang, Column preconcentration of lead in aqueous solution with macroporous epoxy resin-based polymer monolithic matrix, Anal. Chim. Acta, 575 (2006) 166–171.
[51] A.A. Al-Massaedh, M. Schmidt, U. Pyell, U.M. Reinscheid, Elucidation of the enantiodiscrimination properties of a nonracemic chiral alignment medium through gel-based capillary electrochromatography: separation of the mefloquine stereoisomers, ChemistryOpen, 5 (2016) 455–459.
[52] S. Chakraborty, S. Chowdhury, P.D. Saha, Adsorption of crystal violet from aqueous solution onto NaOH-modified rice husk, Carbohydr. Polym., 86 (2011) 1533–1541.
[53] N. Laskar, U. Kumar, Adsorption of crystal violet from wastewater by modified bambusa tulda, KSCE J. Civ. Eng., 22 (2018) 2755–2763.

[54] E. Igberase, P. Osifo, A. Ofomaja, The adsorption of Pb, Zn, Cu, Ni, and Cd by modified ligand in a single component aqueous solution: equilibrium, kinetic, thermodynamic, and desorption studies, Int. J. Anal. Chem., 2017 (2017) 1–15.
[55] D. Robati, Pseudo-second-order kinetic equations for modeling adsorption systems for removal of ammonium ions using multi-walled carbon nanotube, J. Nanostruct. Chem., 3 (2013) 55, doi: 10.1186/2193–8865–3-55.
[56] M.T. Ghaneian, A. Bhatnagar, M.H. Ehrampoush, M. Amrollahi, B. Jamshidi, M. Dehvari, M. Taghavi, Biosorption of hexavalent chromium from aqueous solution onto pomegranate seeds: kinetic modeling studies, Int. J. Environ. Sci. Technol., 14 (2017) 331–340.
[57] Y.S. Ho, G. McKay, Pseudo-second-order model for sorption processes, Process Biochem., 34 (1999) 451–465.
[58] N. Ayawei, A.N. Ebelegi, D. Wankasi, Modelling and interpretation of adsorption isotherms, J. Chem., 2017 (2017), doi: 10.1155/2017/3039817.
[59] S. Liu, Cooperative adsorption on solid surfaces, J. Colloid Interface Sci., 450 (2015) 224–238.
[60] C.H. Giles, D. Smith, A general treatemnt and classification of the solute adsorption isotherm, J. Colloid Interface Sci., 47 (1974) 755–765.
[61] T.S. Anirudhan, S.R. Rejeena, Thorium(IV) removal and recovery from aqueous solutions using tannin-modified poly(glycidylmethacrylate)-grafted zirconium oxide densified cellulose, Ind. Eng. Chem. Res., 50 (2011) 13288–13298.
[62] M.A. Al-Ghouti, D.A. Da'ana, Guidelines for the use and interpretation of adsorption isotherm models: a review, J. Hazard. Mater., 393 (2020) 122383, doi: 10.1016/j.jhazmat.2020.122383.
[63] M. Alaqarbeh, F.I. Khalili, O. Kanoun, Manganese ferrite ($MnFe_2O_4$) as potential nanosorbent for adsorption of uranium(VI) and thorium(IV), J. Radioanal. Nucl. Chem., 323 (2020) 515–537.
[64] I.A.W. Tan, A.l. Ahmad, B.H. Hameed, Adsorption of basic dye on high-surface-area activated carbon prepared from coconut husk: equilibrium, kinetic and thermodynamic studies, J. Hazard. Mater., 154 (2008) 337–346.
[65] O. Hamdaoui, E. Naffrechoux, Modeling of adsorption isotherms of phenol and chlorophenols onto granular activated carbon. Part I. Two-parameter models and equations allowing determination of thermodynamic parameters, J. Hazard. Mater., 147 (2007) 381–394.
[66] G. Limousin, J.-P. Gaudet, L. Charlet, S. Szenknect, V. Barthes, M. Krimissa, Sorption isotherms: a review on physical bases, modeling and measurement, Appl. Geochem., 22 (2007) 249–275.
[67] G. Sharma, Mu. Naushad, Adsorptive removal of noxious cadmium ions from aqueous medium using activated carbon/zirconium oxide composite: isotherm and kinetic modelling, J. Mol. Liq., 310 (2020) 113025, doi: 10.1016/j.molliq.2020.113025.
[68] E.E. Jasper, V.O. Ajibola, J.C. Onwuka, Nonlinear regression analysis of the sorption of crystal violet and methylene blue from aqueous solutions onto an agro-waste derived activated carbon, Appl. Water Sci., 10 (2020)132, doi: 10.1007/s13201-020-01218-y.
[69] D.C.W. Tsang, J. Hu, M.Y. Liu, W. Zhang, K.C.K. Lai, I.M.C. Lo, Activated carbon produced from waste wood pallets: adsorption of three classes of dyes, Water Air Soil Pollut., 184 (2007) 141–155.
[70] U.F. Alkaram, A.A. Mukhlis, A.H. Al-Dujaili, The removal of phenol from aqueous solutions by adsorption using surfactant-modified bentonite and kaolinite, J. Hazard. Mater., 169 (2009) 324–332.
[71] O. Duman, S. Tunç, B.K. Bozoğlan, T.G. Polat, Removal of triphenylmethane and reactive azo dyes from aqueous solution by magnetic carbon nanotube-κ-carrageenan-Fe_3O_4 nanocomposite, J. Alloys Compd., 687 (2016) 370–383.
[72] O. Duman, S. Tunç, T.G. Polat, Determination of adsorptive properties of expanded vermiculite for the removal of C. I. Basic Red 9 from aqueous solution: kinetic, isotherm and thermodynamic studies, Appl. Clay Sci., 109–110 (2015) 22–32.